



UNIVERSITY OF LEEDS

This is a repository copy of *Facile Synthesis of Perovskite-Structured Powders Using Barite–Celestite Ore under Hydrothermal Alkaline Conditions*.

White Rose Research Online URL for this paper:
<http://eprints.whiterose.ac.uk/120914/>

Version: Accepted Version

Article:

Rendón-Angeles, JC, Matamoros-Veloza, Z, Matamoros Veloza, A et al. (3 more authors) (2017) Facile Synthesis of Perovskite-Structured Powders Using Barite–Celestite Ore under Hydrothermal Alkaline Conditions. *Industrial & Engineering Chemistry Research*, 56 (36). pp. 9942-9952. ISSN 0888-5885

<https://doi.org/10.1021/acs.iecr.7b02383>

© 2017 American Chemical Society. This document is the unedited Author's version of a Submitted Work that was subsequently accepted for publication in *Industrial & Engineering Chemistry Research*, copyright © American Chemical Society after peer review. To access the final edited and published work see <https://doi.org/10.1021/acs.iecr.7b02383>.

Reuse

Items deposited in White Rose Research Online are protected by copyright, with all rights reserved unless indicated otherwise. They may be downloaded and/or printed for private study, or other acts as permitted by national copyright laws. The publisher or other rights holders may allow further reproduction and re-use of the full text version. This is indicated by the licence information on the White Rose Research Online record for the item.

Takedown

If you consider content in White Rose Research Online to be in breach of UK law, please notify us by emailing eprints@whiterose.ac.uk including the URL of the record and the reason for the withdrawal request.



eprints@whiterose.ac.uk
<https://eprints.whiterose.ac.uk/>

Facile Synthesis of Perovskite-Structured Powders Using Barite–Celestite Ore under Hydrothermal Alkaline Conditions

Juan C. Rendón-Angeles[†], Zully Matamoros-Veloza[‡], Adriana Matamoros Veloza[§], Roberto Perez-Garibay[†], José L. Rodríguez-Galicia[†], and Yanagisawa Kazumichi[¶]

[†] Department of Ceramic Engineering, Research Center for Advanced Studies of the NPI, Saltillo-Campus, Ramos Arizpe, 25900 Coah, México

[‡] Faculty of Engineering Saltillo, Saltillo Institute of Technology, 25820 Coahuila, México

[§] Institute of Thermofluids, School of Mechanical Engineering, University of Leeds, Leeds LS2 9JT, United Kingdom

[¶] Research Laboratory for Hydrothermal Chemistry, Kochi University, Akebono, Kochi, 780-8520, Japan

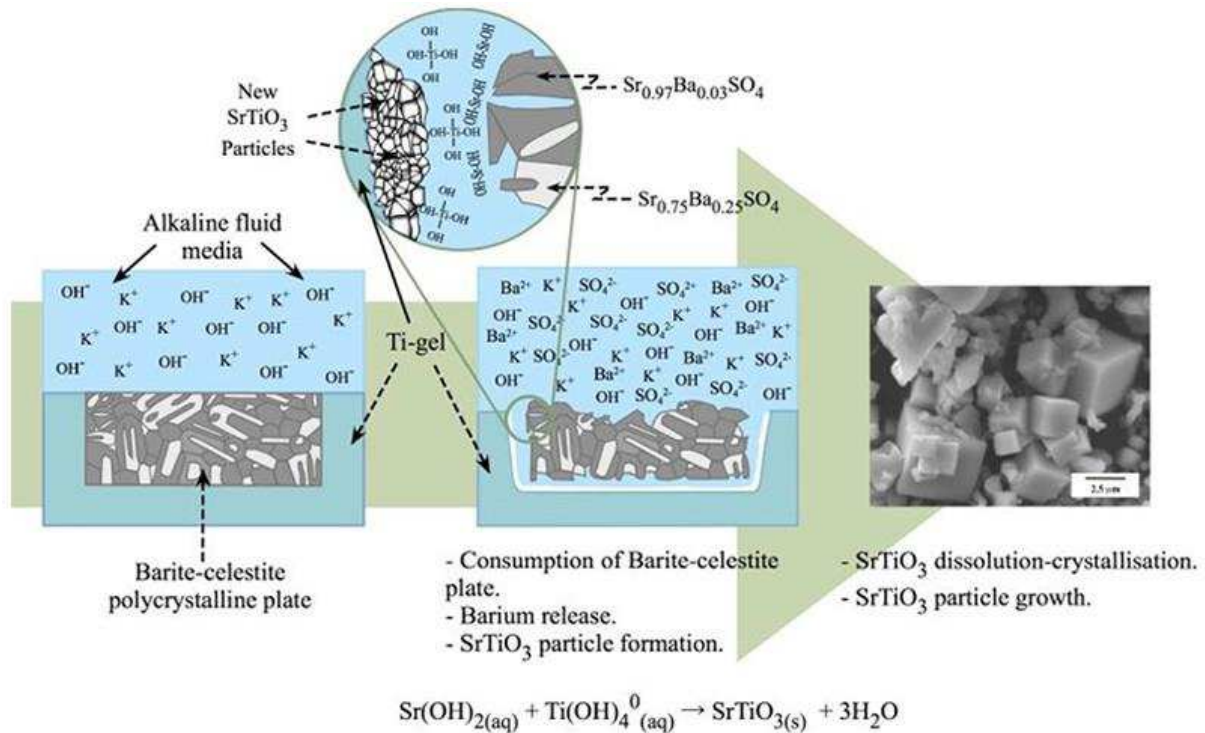
Ind. Eng. Chem. Res., Article ASAP

DOI: 10.1021/acs.iecr.7b02383

*E-mail: jcarlos.rendon@cinvestav.edu.mx.

Abstract

Barite–celestite (BC) crystals were treated in highly concentrated alkaline hydrothermal fluid (5 M KOH) coexisting with a $\text{Ti}(\text{OH})_4 \cdot 4.5\text{H}_2\text{O}$ gel to produce SrTiO_3 particles between 150 and 250 °C for several intervals between 6 h and 96 h. The BC transformation was initiated at a lower temperature (150 °C) and the total precursors consumption was completed at 250 °C for 96 h, resulting only in the crystallization of SrTiO_3 particles. Different temperatures of reaction (≤ 200 °C) lead to variations in morphology and particle size of the SrTiO_3 . The crystal growth of faceted cubic agglomerates was achieved at 250 °C, and it is provoked by the Oswald ripening mechanism. The release of barium to the hydrothermal fluid from the precursor occurred simultaneously with the transformation process. A low value of activation energy required for the single-step transformation of the BC plates into SrTiO_3 particles was observed (26.33 kJ mol⁻¹), under static hydrothermal conditions.



One-step hydrothermal transformation processing of barite-celestite crystals into SrTiO₃ particles

1 Introduction

Recently, increasing attention has been paid to the synthesis and characterization of perovskite materials [e.g., SrTiO₃ (STO), BaTiO₃ (BTO)] and their solid solutions [i.e., Ba_{1-x}Sr_xTiO₃ (BSTO)], because of their large nonlinear optical coefficient and dielectric constants. The STO is an indirect band gap semiconductor with a band gap of 3.4 eV(1) and has high thermal and chemical stability and a low thermal expansion coefficient, which are attractive features for a broad range of applications, including catalysts,(2, 3) electronics, and optoelectronics.(4-6) However, these characteristics are dependent on particle size, morphology, crystalline structural defects, and surface properties, which are defined by the conditions used in the synthesis method. The typical methods used to prepare either BSTO or STO involve high temperature via solid-state reaction,(7) combustion,(4) molten salt,(8-10) and pyrolysis;(11) however, recently, low-temperature soft chemical methods(1-3, 12) such as sol-gel,(13, 14) chemical coprecipitation,(15) and liquid-solid reactions, are being used, because of their simplicity, low cost, and environmentally friendly nature.

Soft chemistry routes such as the hydrothermal processing have been widely used to prepare BTO(16, 17) or STO(18-23) particles with controlled sizes and specific morphologies by determining the optimal conditions of temperature and pH of the hydrothermal fluid.(24) Similarly, the use of different precursors (e.g., Ti-gel,(25) TiO₂ powders,(22, 26) and strontium (Sr(NO₃)₂

salt) influences control of the crystallization process of cubic perovskite titanates. Some of the present authors have previously explored the use of high-purity sulfate mineral ores (i.e., SrSO₄ as precursor mineral) for preparing inorganic compounds (i.e., SrCO₃(27) and SrF₂(28)) via a single-step conversion. The solubility of SrSO₄ mineral plays an important role to complete the conversion under alkaline fluids under hydrothermal conditions, because the solubility of the mineral hinders its dissolution, even in mild alkaline hydrothermal media (<1 M KOH).(29) The first evidence of the preparation of STO powders via the single-step transformation was reported by Rangel-Hernandez,(30) who studied the formation of STO particles exhibiting different particle size (0.2–6 μm) and morphologies (peanut-like and pseudo-cubic) during the processing of a SrSO₄ ore polycrystalline plate embedded into Ti(OH)₄·4.5H₂O gel in a highly concentrated KOH solution (5 M). The complete dissolution of the crystal plate occurred in a single step without the formation of secondary phases at 250 °C for 96 h, and the kinetic studies indicated that this reaction requires an activation energy of 27.9 kJ mol⁻¹.(30) In this case, the formation of STO particles is triggered by a massive dissolution of both SrSO₄ plate and Ti-gel in the highly concentrated alkaline media. Consequently, the fluid saturation in solute produced the nucleation and subsequent crystal growth. Hence, the hydrothermal processing is a technique applicable to transform other low-cost mineral species (i.e., BC) to produce a perovskite-structured functional powders.

Barite–celestite mineral (hereafter referred as BC) is a mineral composed by a solid-solution series of SrSO₄ (celestite) and BaSO₄ (barite), the most common solid solution (Sr_{1-x}Ba_xSO₄), is found in highly pure celestite mineral reservoirs. This mineral ore is constituted by ~65 wt % of SrSO₄ containing barium as a major impurity and Ca in minor concentrations.(31) This mineral species has low commercialization value and it is commonly used for landfill purposes. Hence, in the present work, we investigate the use of this low-cost mineral to prepare functional perovskite structured compounds. The chemical reactivity and the reaction pathway toward the crystallization of perovskite structure of BSTO or STO were studied under high alkaline hydrothermal conditions. Hence, in the present work, we have directed our effort toward determining the feasibility for employing this low-cost mineral resource that contains two valuable elements, Sr and Ba, as a raw material for preparing functional perovskite-structure compounds. The chemical reaction pathway of the BC crystals, the aspects of the synthesized STO powders (including particle size, morphology, and crystalline phase), and the kinetics associated with the single-step reaction were also investigated.

2 Experimental Procedure

2.1 Precursor Material Preparation

2.1.1 Barite–Celestite (BC)

Crystalline barite–celestite aggregates (BC, $\text{Sr}_{1-x}\text{Ba}_x\text{SO}_4$) were collected from a mineral reservoir in northeast Mexico in the Coahuila State. BC polycrystalline plates were obtained from the raw mineral by cutting square plates with dimensions of 6 ± 1 mm side and 2 ± 0.5 mm thick, using a diamond disk cutter machine. The plates were rinsed with deionized water and sonicated. Preliminary powder X-ray analysis of the BC plates (Figure 1a) revealed that the mineral belongs to orthorhombic system with Pnma space group (JCPD File No. 05-0593); however, the major peaks exhibited a slight displacement from the peak positions of pure SrSO_4 mineral constituted by a low content of impurities (JCPD File No. 05-0593, <0.11 wt %; such as <0.1 wt % Ba, <0.01 wt % Na, <0.001 wt % Al). The displacement of the X-ray diffraction (XRD) peaks of the BC sample employed for the experiments in the present work is attributed to the incorporation of a large amount of Ba^{2+} ions. The wet chemical analyses of the BC plates confirmed that Sr (31.78 wt %), Ba (19.52 wt %), SO_4^{2-} (48.77 wt %), and CO_3^{2-} (0.60 wt %) are the major constituents; these contents correspond to 61.42 wt % SrSO_4 , 36.58 wt % BaSO_4 , and 1.4 wt % SrCO_3 . Low amounts (<0.6 wt %) of Ca, Na, Fe, and K were also determined as impurities in the plates. Furthermore, microstructural analyses conducted by scanning electron microscopy (SEM) indicated that the BC feedstock was constituted by two randomly distributed phases (see Figure 1a). Microprobe punctual EDX analyses conducted in Areas 1 (light) and 2 (dark) in the plate revealed the chemical composition of two mineral phases (Figure 1b). According to the EDX analyses, the light region (Area 1) corresponds to the solid solution of $\text{Sr}_{0.75}\text{Ba}_{0.25}\text{SO}_4$, and the dark region (Area 2) corresponds to the strontium-rich $\text{Sr}_{0.97}\text{Ba}_{0.03}\text{SO}_4$ phase.

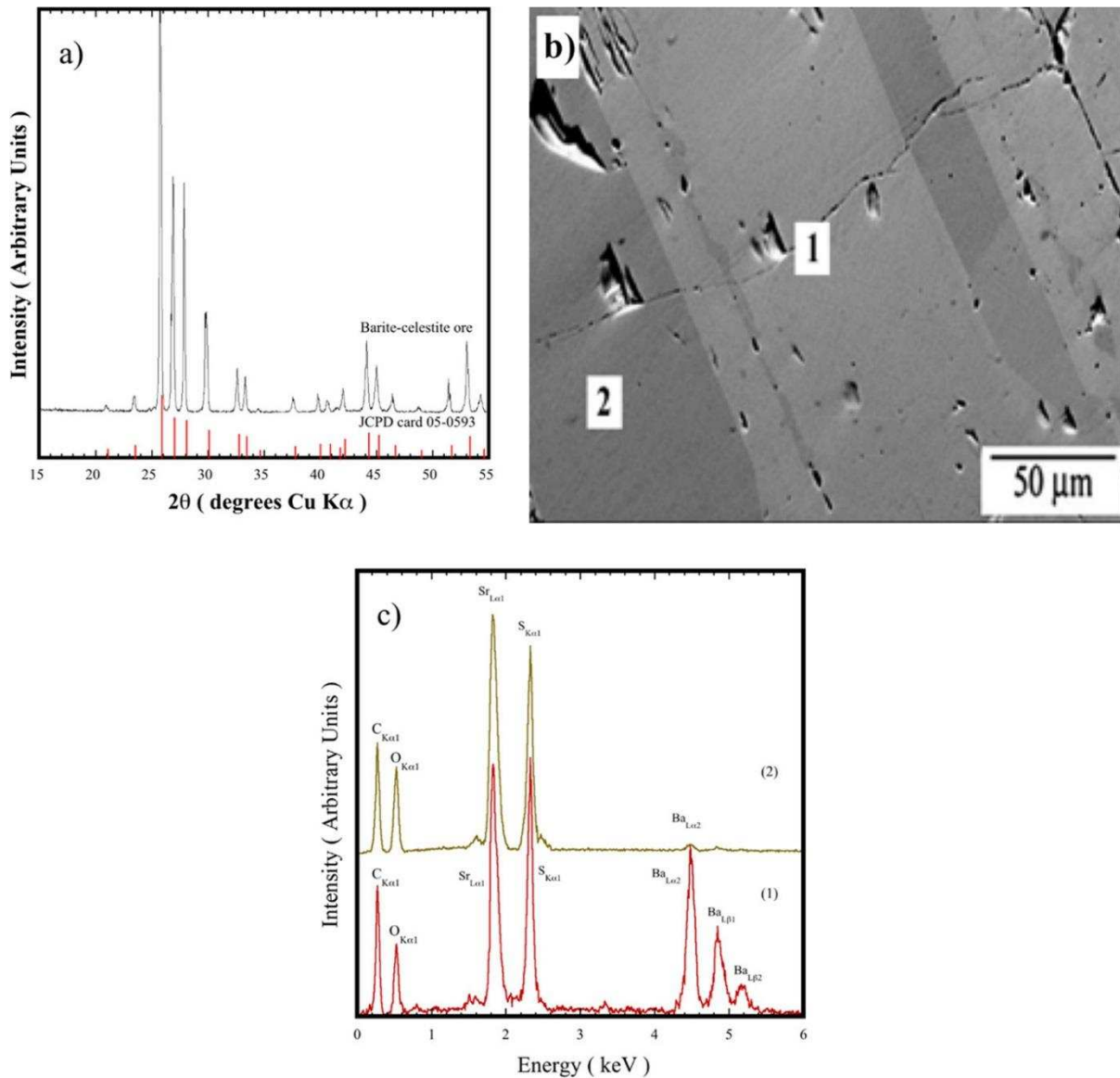


Figure 1. (a) X-ray diffraction (XRD) pattern of powdered BC mineral ore. (b) Microstructure aspects revealed on the polished surface of the barite–celestite (BC) polycrystalline plate; and (c) punctual EDX analyses spectrum obtained at the light zone indicated in the micrograph (denoted as “1”) and the dark area indicated in the micrograph (denoted as “2”).

2.1.2 Titanium Gel

Titanium hydroxide gel (Ti-gel) was selected as a Ti source and was prepared following the procedure reported elsewhere.⁽²²⁾ The chemical composition of the precursor gel was determined via thermogravimetric analysis, coupled with differential thermal analysis (TG/DTA) conducted in air up from 25 °C to 1000 °C at a heating rate of 5 °C/min, using a Seiko Model SSC5200 instrument. The chemical formula of the as-prepared Ti-gel was determined as $\text{Ti}(\text{OH})_4 \cdot 4.5\text{H}_2\text{O}$.

2.2 Hydrothermal Treatments

A BC plate of 0.2 and 1 g of Ti-gel were placed at the bottom of a Teflon-lined stainless steel vessel autoclave. The amounts of the reactant precursors were mixed to yield 1 mol of $\text{Sr}_{1-x}\text{Ba}_x\text{TiO}_3$ or SrTiO_3 . The feasibility for preparing other compounds in the BaTiO_3 – SrTiO_3 binary system, as the major reaction product (BSTO) was investigated via detailed analysis of the reaction pathway. Therefore, the objective of the treatments that were performed was to elucidate the effect of temperature and reaction interval on the transformation of the precursors to the perovskite-structured compound. Note that the effect of the concentration of the alkaline media was not studied, because the solubility of sulfate compounds decreases drastically in alkaline solutions with concentrations below 5 M (MOH, where M = Na, K). (30) All the hydrothermal treatments were conducted by employing a 5 M KOH solution and a volume of 27 mL that corresponds to an inner vessel filling ratio of 40%. The autoclaves were sealed and placed in a forced-air convection oven, which was then heated to the selected reaction temperature (150–250 °C) and maintained for several reaction intervals (3–96 h). After the hydrothermal treatment, the reaction products were separated from the remaining solution, rinsed, and sonicated with deionized water.

2.3 Characterization of the Reaction Products

Powder XRD analyses were performed to identify the crystalline phases of the reaction products by using an X-ray diffractometer (Rigaku, Model RTP-300RC) with graphite-monochromatized Cu K α radiation ($\lambda = 1.54056 \text{ \AA}$) at 40 kV and 100 mA. The diffraction patterns were collected between 10° and $80^\circ 2\theta$, at a scanning speed of $4^\circ/\text{min}$ in a $2\theta/\theta$ scanning mode with a 0.02° step. Lattice parameter a was calculated via the least-squares method, using Si as an internal standard. The morphology of the particles was observed by scanning electron microscopy (SEM) (Phillips, Model XL30 ESEM), and EDX analyses on 10 different spots were conducted to quantify the Sr and Ti atomic content. Particle size was calculated from 50 particles observed in the SEM images. Wet chemical characterization was conducted by inductively coupled plasma-atomic emission spectrometry (ICP-AES) (Model Multitype I ICP-9000, Shimadzu, Japan), to determine the barium content in the solution on the samples prepared at 150 and 250 °C. An aliquot of 1 mL was diluted to 100 mL, using a 1 M HNO_3 solution. Three different solutions, containing 5, 10, and 50 ppm of Ba, were prepared, using a reagent-grade Ba standard solution (Wako Chemical, 1000 ppm). These solutions were employed to calibrate the ICP apparatus prior to the analysis of the solutions that remained after the hydrothermal treatments.

The kinetics related to the consumption of BC plates and the simultaneous formation of perovskite-structured powders was evaluated using the shrinking core (“SC”) model for solid–liquid systems reported elsewhere. (32, 33) This model considers a bulk solid dissolution step that occurs in the liquid phase, analogous to the chemical equilibrium related to the transformation of the BC ore into SrTiO_3 in this study. The SC model assumes that the reaction rate (r) of the solid BC plate is controlled by the chemical reaction at the solid surface coupled with the diffusion

through a solution boundary layer. Therefore, as a function of the consumption ratio (α), the reaction rate can be written as follows:

$$r = \frac{d}{dt} = kf(\alpha) \quad (1)$$

where k is the reaction rate constant and $f(\alpha)$ is the function for the solid consumption. If we considered that W_{BC} is the weight of the remaining BC plate and W_{IST} is the weight of the SrTiO_3 product, then the fraction of mineral BC consumed (α) can be determined at any reaction interval selected by using the expression $\alpha = 1 - W_{\text{BC}}$ or $\alpha = W_{\text{IST}}$. The consumption ratio (α) of BC plate for each experimental hydrothermal treatment was determined using the remaining weight of the BC plate. The rate constant (k) was then determined from linear regression of the data portrayed in the $\ln(1 - \alpha)$ vs t plots. This particular expression make use of the empirical kinetic laws, in which $f(\alpha) = (1 - \alpha)^n$, where n is a reaction order. This approach allows calculation of various empirical functions to fit the kinetics and helps deduce the reaction mechanism that occurs at the solid/liquid interface.(33) In the present work, the rate constant (k) was calculated via the first-order kinetics; this function fitted the experimental data well among other equations related with the dissolution kinetics of solid–liquid systems, and this model is in good agreement with the results reported by Markus et al.(32) The activation energy (E_a) was calculated with the Arrhenius equation, using linear regression. The activation energy associated with the equilibrium, regardless of the dissolution of bulk BC ore in an alkaline solution and the crystallization of the perovskite powders, was determined for the current system.

3 Results and Discussion

3.1 Structural Aspects of the Perovskite Powders via the Transformation of Polycrystalline BC

The hydrothermal treatments of BC plates are focused on evaluating the effect of reaction interval and temperature on the reaction rates, crystallinity, and morphology; however, in all of the experiments conducted, the transformation led to the crystallization of a single perovskite-structured phase (SrTiO_3). In this set of experiments, the formation of SrTiO_3 proceeded by a gradual dissolution of both the BC plate and the Ti-gel precursors in the KOH solution, and we observed after the treatments that the reaction was uncomplete leaving unreacted precursors at the bottom of the reactor. The powders obtained as the main reaction product were separated from the partially reacted products (BC plate and Ti-gel) on all of the experiments where the reaction did not conclude, and the SrTiO_3 particles were well-cleaned prior the EDX compositional analyses. Table 1 summarizes a selection of various experimental conditions and details of the lattice parameters of the precipitate phase (SrTiO_3), and the presence of the

remaining precursor compounds is included in Table 1, for the experiments conducted at low temperature and short reaction intervals.

Table 1. Summary of the Hydrothermal Treatments Conducted for Studying the Conversion of Barite–Celestite (BC) Plates into SrTiO₃

| sample | temperature (°C) | time (h) | crystalline phases and unreacted precursors ^a | lattice parameter a (Å) | cell volume (Å ³) | Elemental Content | |
|--------|---------------------|-------------|--|----------------------------|----------------------------------|--------------------------|--------------------------|
| | | | | | | Sr ²⁺ (at. %) | Ti ⁴⁺ (at. %) |
| ST1 | 250 | 6 | BC, ^a Ti-gel, ^a SrTiO ₃ , SrCO ₃ | 3.9123(3) | 59.882(6) | 48.38 (0.7) | 51.62 (0.7) |
| ST2 | 250 | 12 | BC, ^a Ti-gel, ^a SrTiO ₃ | 3.9113(4) | 59.512(7) | | |
| ST3 | 250 | 24 | BC, ^a Ti-gel, ^a SrTiO ₃ | 3.9102(3) | 59.789(7) | 48.30 (0.9) | 51.70 (0.9) |
| ST4 | 250 | 48 | BC, ^a Ti-gel, ^a SrTiO ₃ | 3.9069(3) | 59.636(6) | 51.04 (0.9) | 48.96 (0.9) |
| ST5 | 250 | 72 | BC, ^a Ti-gel, ^a SrTiO ₃ | 3.9142(5) | 59.970(7) | 48.64 (0.9) | 51.36 (0.9) |
| ST6 | 250 | 96 | SrTiO ₃ | 3.9110(1) | 59.827(8) | 49.79 (0.9) | 50.21 (0.9) |
| ST7 | 200 | 6 | BC, ^a Ti-gel, ^a SrTiO ₃ , SrCO ₃ | 3.9174(6) | 60.118(3) | 49.47 (0.3) | 50.53 (0.3) |

| sample | temperature (°C) | time (h) | crystalline phases and unreacted precursors ^a | lattice parameter a (Å) | cell volume (Å ³) | Elemental Content | |
|--------|---------------------|-------------|--|----------------------------|----------------------------------|--------------------------|--------------------------|
| | | | | | | Sr ²⁺ (at. %) | Ti ⁴⁺ (at. %) |
| ST8 | 200 | 24 | BC, ^a Ti-gel, ^a SrTiO ₃ , SrCO ₃ | 3.9159(3) | 60.048(8) | 49.39 (0.5) | 50.61 (0.5) |
| ST9 | 200 | 48 | BC, ^a Ti-gel, ^a SrTiO ₃ , SrCO ₃ | 3.9195(6) | 60.214(7) | | |
| ST10 | 200 | 72 | BC, ^a Ti-gel, ^a SrTiO ₃ | 3.9220(5) | 60.332(9) | 47.11 (0.7) | 52.89 (0.7) |
| ST11 | 200 | 96 | BC, ^a Ti-gel, ^a SrTiO ₃ | 3.9193(8) | 60.207(9) | 48.11 (0.5) | 51.89 (0.5) |
| ST12 | 150 | 12 | BC, ^a Ti-gel, ^a SrTiO ₃ , SrCO ₃ | 3.9300(10) | 60.703(7) | 50.13 (0.3) | 49.87 (0.3) |
| ST13 | 150 | 48 | BC, ^a Ti-gel, ^a SrTiO ₃ , SrCO ₃ | 3.9208(3) | 60.277(9) | | |
| ST14 | 150 | 72 | BC, ^a Ti-gel, ^a SrTiO ₃ , SrCO ₃ | 3.9130(4) | 59.918(8) | 48.39 (0.6) | 51.61 (0.6) |
| ST15 | 150 | 96 | BC, ^a Ti-gel, ^a SrTiO ₃ , SrCO ₃ | 3.9202(6) | 60.249(9) | 49.21 (0.7) | 50.79 (0.7) |

| | | | | | | Elemental Content | |
|--------|-------------|------|--|-------------------------|-------------------------------|--------------------------|--------------------------|
| sample | temperature | time | crystalline phases and unreacted precursors ^a | lattice parameter a (Å) | cell volume (Å ³) | Sr ²⁺ (at. %) | Ti ⁴⁺ (at. %) |
| | (°C) | (h) | | | | | |
| | | | strontium titanate (SrTiO ₃) ^b | 3.905 | 59.550 | | |

a Partially reacted precursors found at the bottom of the autoclave after the hydrothermal treatment; these were separated gravimetrically from the primary reaction product SrTiO₃ particles.

b Strontium titanate (tousinite), JCPDS File No. 35-0734.

Under alkaline hydrothermal conditions, the hydrolysis of the BC precursor containing Ba and Sr might promote the synthesis of Sr_{1-x}Ba_xTiO₃ powders; however, the crystallization of this perovskite compound is highly dependent on the dissolution of the BC feedstock. This inference is supported by the fact that other related sulfate minerals (i.e., celestite) dissolve rapidly in alkaline solution (5 M KOH) under hydrothermal conditions.⁽³⁰⁾ However, the dissolution of the mineral is limited by the presence of other compounds such as Ti(OH)₄ gel, which globally causes a reduction of the speed of the transformation of SrTiO₃ particles in the hydrothermal system.

In addition, the content of Sr and Ti in the newly SrTiO₃ powders measured by punctual electron microprobe X-ray energy-dispersive spectroscopy (EDX) analyses are given also in Table 1 for comparison. Generally, the lattice parameter a of the SrTiO₃ agree between the different treatments and that reported in JCPDS File No. 35-0734; however, small variation in the value of a might be attributed to either lattice distortions or residual stress induced in the unit cell during the crystallization stage. Structural strain is likely promoted by even small variations in the experimental parameters, reaction time and temperature, and processing route.^(34, 35)

Figure 2 shows the crystalline structural parameters of products obtained from the hydrothermal treatments listed in Table 1. XRD patterns confirmed the formation of a major phase composed of SrTiO₃, matching JCPDS File No. 35-0734 with a perovskite-type cubic structure. The formation of SrTiO₃ powder occurred even at very short reaction intervals (i.e., 6 h; see Figure 2a) with partial consumption of the BC plate, and full conversion was achieved at 250 °C for 96 h.

The formation of SrTiO₃, also occurred at a low temperature (150 °C), and the increase of treatment temperature produced a rapid dissolution of both constituent phases in the BC plate, producing higher amounts of SrTiO₃ (Figure 2b). The XRD structural analyses indicated the formation of SrCO₃ (JCPDS File No. 05-0418) as a byproduct at all temperatures studied and short reaction times (6 or 12 h; see Table 1); its formation likely results from the reaction between gaseous CO₂, adsorbed from the atmosphere; and KOH in solution. The crystallization of SrCO₃ was previously documented by Mourão et al.,(36) who obtained it under similar conditions of SrTiO₃ particle synthesis as observed in this work, and explained that the formation of SrCO₃ occurred because of its low solubility product ($K_{sp} = 9.3 \times 10^{-10}$ at 25 °C) under alkaline hydrothermal conditions at mild temperatures.

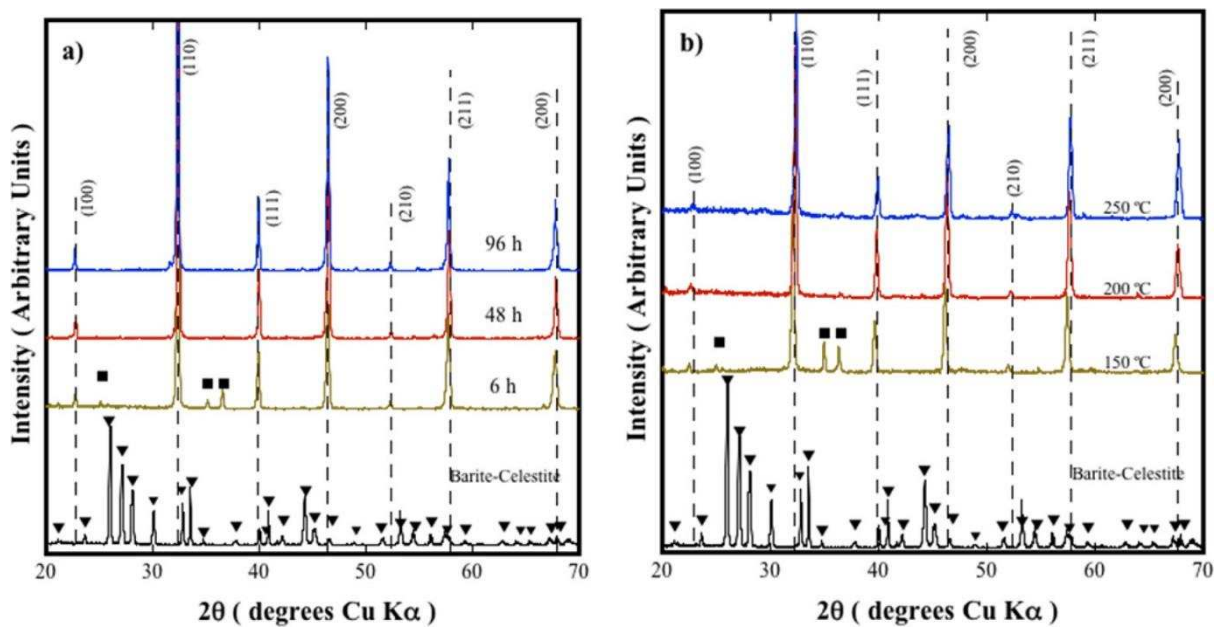


Figure 2. XRD patterns of the reaction products obtained after the hydrothermal treatment of BC polycrystalline plates conducted in a 5 M KOH solution (a) at 250 °C for several reaction intervals and (b) for 12 h at different temperatures. Miller indexes correspond to SrTiO₃ with a perovskite cubic structure. [Symbol legend: (▼) BC ore and (■) SrCO₃ reaction byproduct.]

3.2 Compositional Aspects of the SrTiO₃ Powders and Barium Dissolution

EDX analyses conducted on the powders prepared under various conditions of temperature (Figure 3a) and reaction time (Figure 3b), confirmed that strontium and titanium were the only elements present in the SrTiO₃ powders. The composition of these elements was estimated using the ZAF correction routine from 10 individual point analyses, which were similar in all cases, indicating a highly SrTiO₃ precipitate. The quantitative Sr and Ti contents are almost similar to that of the stoichiometric SrTiO₃ compound that contains 50 at. % Sr and 50 at. % Ti.

Interestingly, the typical EDX spectra of SrTiO₃ powders hydrothermally crystallized by the complete conversion of BC plates at 250 °C for 24 h showed no detectable levels of impurities incorporated in the perovskite crystalline structure, such as barium, sulfur, or potassium (see Figure 3). This compositional analysis also confirmed that Ba²⁺ ions were not incorporated in the structure of the SrTiO₃ particles during the synthesis process. Therefore, this result indicates that Ba²⁺ ions were gradually hydrolyzed in the hydrothermal media as the reaction progressed and remained in solution.

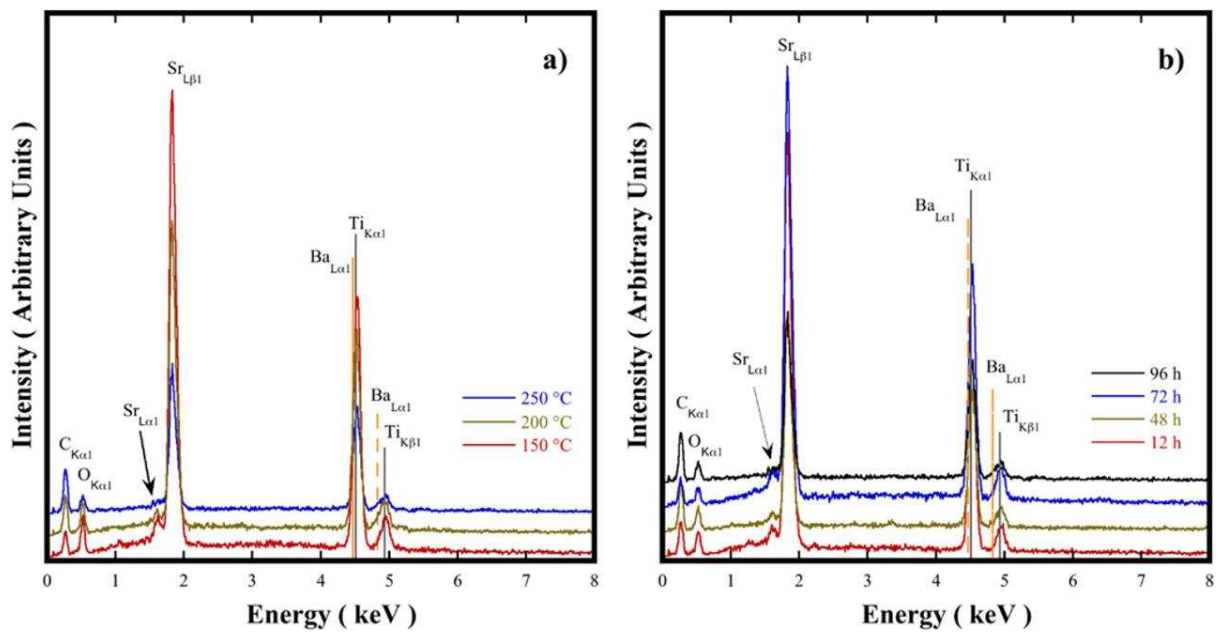


Figure 3. EDX spectrum of the various SrTiO₃ particles obtained under hydrothermal conditions using 5 M KOH solutions (a) for 96 h at different temperatures and (b) at 200 °C for different reaction intervals.

Figure 4 shows the variation of Ba²⁺ content determined by wet chemical analyses conducted by inductively coupled plasma (ICP) spectrometry on the remnant fluid from treatments conducted at 150 and 250 °C in a 5 M KOH solution for several reaction intervals. Generally, the fraction of Ba dissolved (x) from the BC plate exhibited an exponential increase as a function of the reaction time, and this behavior is marked in the treatments conducted at 250 °C. At both temperatures, the gradual massive dissolution of the BC plate occurring under hydrothermal conditions provoked the release of Ba, and this element was simultaneously hydrolyzed in the hydrothermal media. A total Ba fraction of $x = 0.98$ was obtained after 96 h of conversion, and this value corresponds to a Ba content of 19.1 wt %, which is similar to the initial Ba content (19.52 wt %). Furthermore, the crystallization of other Ba crystalline phases (i.e., Ba(OH)₂) did not occur simultaneously with the SrTiO₃ powder, because the Ba(OH)₂ is highly soluble in water (0.33 mol/kg H₂O). This fact produced the formation of BaOH⁻ species in the alkaline media (5 M KOH), and the BaOH⁻ ionic species is chemically stable under hydrothermal conditions, even

when low barium contents in highly concentrated alkaline media are added. In fact, this has been experimentally demonstrated in the hydrothermal synthesis of BaTiO_3 powders using highly concentrated alkaline media.(37) Moreover, the BaOH^- species is thermodynamically stable at $\text{pH} > 12$,(37) preventing the formation of an intermediate solid solution phase (e.g., $\text{Sr}_{0.72}\text{Ba}_{0.28}\text{TiO}_3$) in the present reaction system, and the ICP analyses conducted at two different temperatures support this inference.

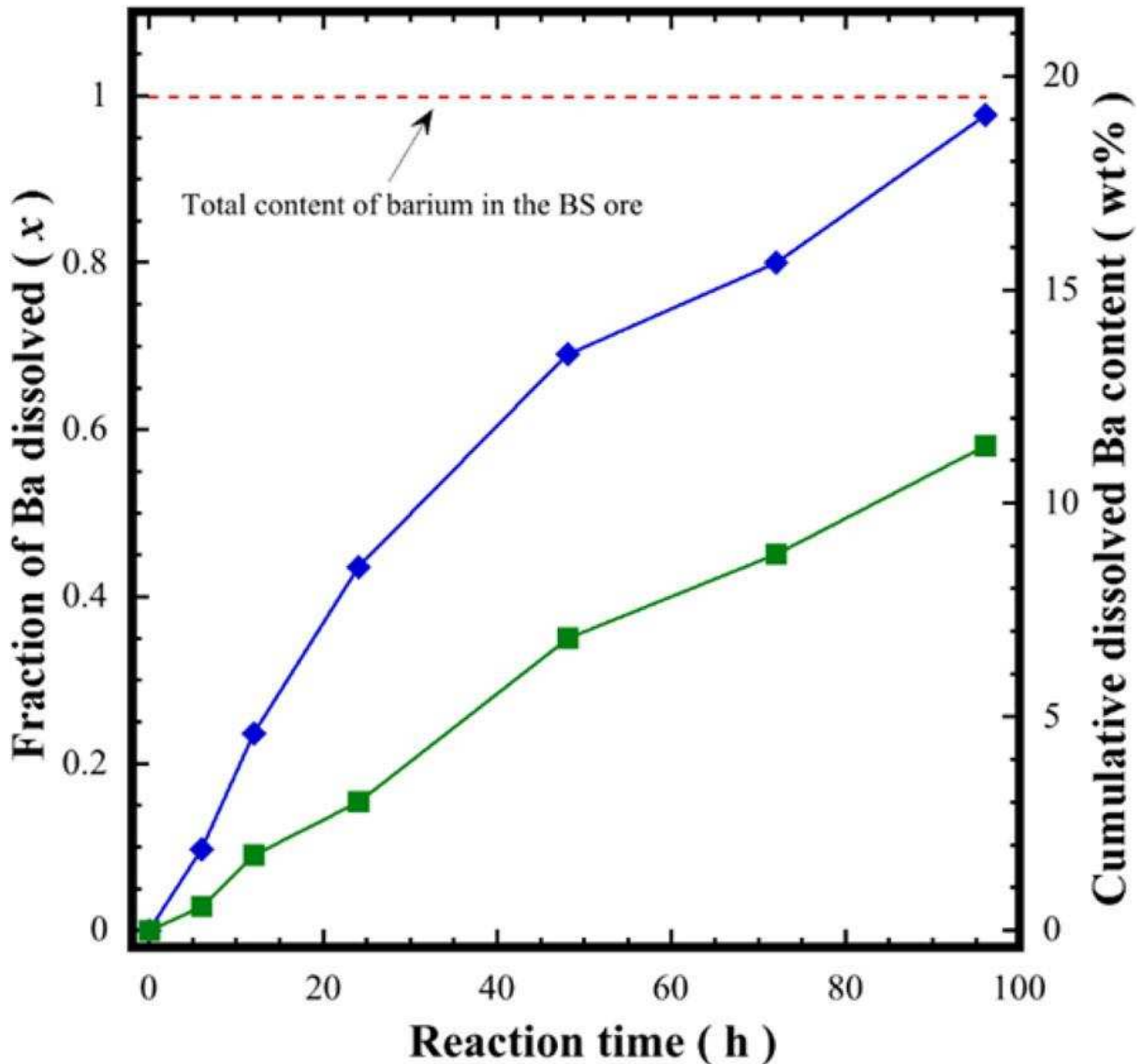


Figure 4. Variation of Ba content determined in the hydrothermal fluid after the conversion of BC polycrystalline plates into SrTiO_3 powders conducted at two different temperatures ((■) 150 and (◆) 250 °C) in a 5 M KOH solution for several reaction intervals.

3.3 Morphology of the Hydrothermally Synthesized SrTiO_3 Powders

Figure 5 shows the morphologies of the SrTiO_3 particles produced from the conversion of BC plates performed at 250 °C in a 5 M KOH solution for various reaction intervals. Generally, the observations indicate that a gradual increase in the size of SrTiO_3 occurred as the time of

reaction increased. Cubic-shaped SrTiO_3 particles $<2.5 \mu\text{m}$ in size were observed after 6 h of reaction; however, few particles resembling dendritic and irregular (noneuhedral) morphologies, as well as some with long prismatic crystals, were also observed (see Figure 5a). The latter large particles were identified as SrCO_3 , because Ti is not incorporated in these particles, as suggested by the Ti K α mapping conducted via EDX analysis (Figure 5b); this inference is supported by the XRD results (Figure 2a) that indicate the large SrCO_3 particles were formed simultaneously with the SrTiO_3 particles. When the treatment was performed for 24 h, regular cubic SrTiO_3 particles were produced ($\sim 3.0 \mu\text{m}$ in size), and these crystals exhibited a marked agglomeration (Figure 5b). A reduced number of small SrTiO_3 particles ($0.9 \mu\text{m}$ in size) with irregular shape also were present. In this process, at $250 \text{ }^\circ\text{C}$, the reaction rates are inferred to have been fast at long treatment intervals. At 48 h, a slight growth of the SrTiO_3 cubic agglomerates and the crystallization of a significant volumetric fraction of elongated irregular-shaped particles $\sim 1.0 \mu\text{m}$ in size occurred. Interestingly, the small cubic particles that formed after 6 h of reaction disappeared; they likely dissolved while achieving the growth of the SrTiO_3 agglomerates (Figure 5c). After full consumption of both precursors (i.e., 96 h reaction), the volumetric fraction of larger cubic crystals and typical perovskite crystals(38) increased significantly and the proportion of small particles was further reduced (Figure 5d).

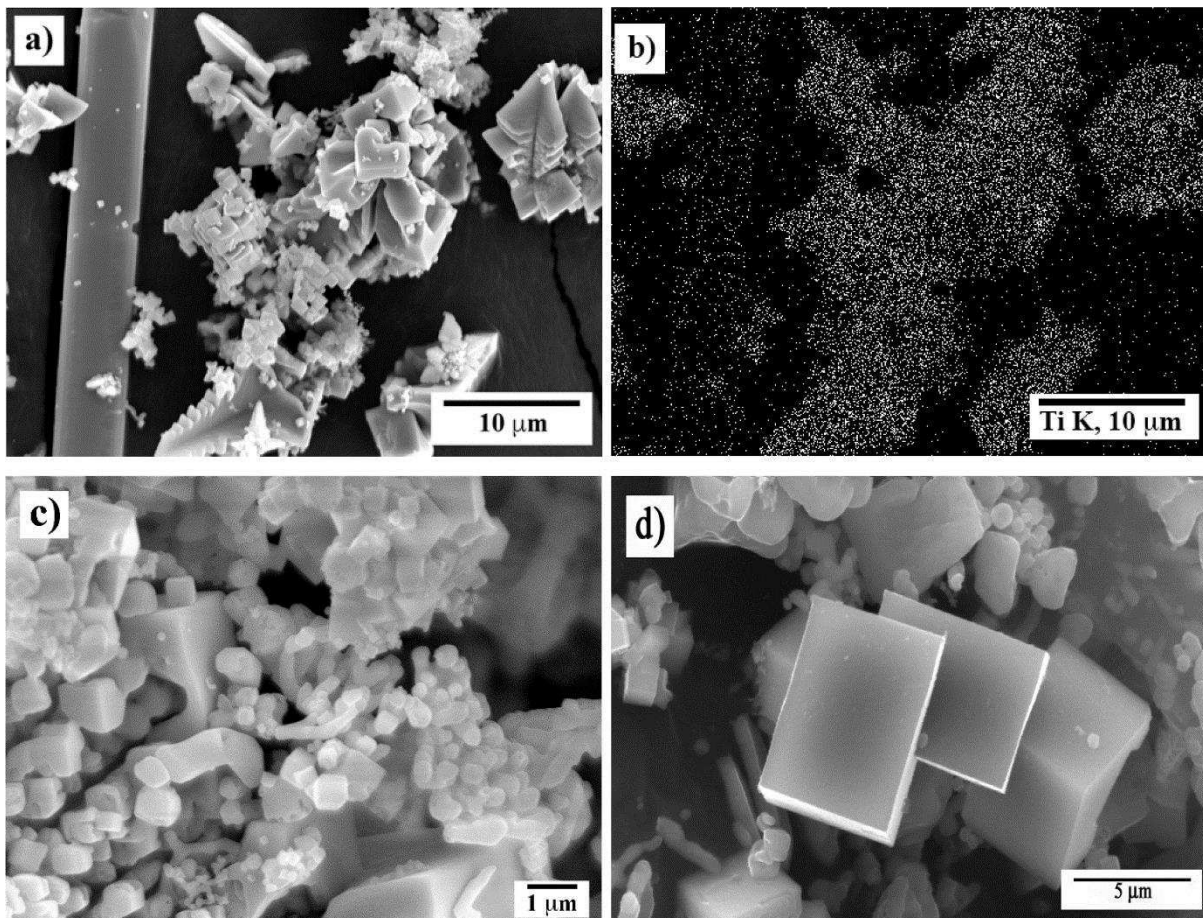


Figure 5. SEM images of the SrTiO₃ particles obtained after hydrothermal treatments of the BC plates in a 5 M KOH solution reacted at 250 °C for (a) 6, (c) 48, and (d) 96 h. Panel (b) shows an EDX mapping analysis (Ti K radiation).

SEM images from products of the hydrothermal synthesis at a fixed time of reaction of 96 h and at various temperatures are shown in Figure 6. Generally, when the treatment was carried out at low temperature (150 °C), the presence of cubic-shaped particles with a bimodal size distribution was observed. The occurrence of large particles (1.5–4.5 μm in size) seems to be low, while the small SrTiO₃ particles (0.5–1.0 μm) are abundant (see Figure 6a). Increasing the temperature up to 200 °C led to the formation of cubic and a few star-shaped particles with an apparent homogeneous particle size distribution in the range of 1.2–6.5 μm (see Figure 6b). At this temperature, evidence of particle growth was not observed; however, when increasing the temperature to 250 °C, a remarkable crystal growth of the SrTiO₃ particles was observed, reaching up to 6 μm in size (Figure 6c). These particles formed large bulky agglomerates (20 μm average size) provoked by a faceted growth process. The randomly distributed faceted SrTiO₃ particles grew on those particle surfaces with a low surface tension, such as flat, smooth, and angular surfaces,(40) and occurred in the process investigated as suggested in Figure 5c.

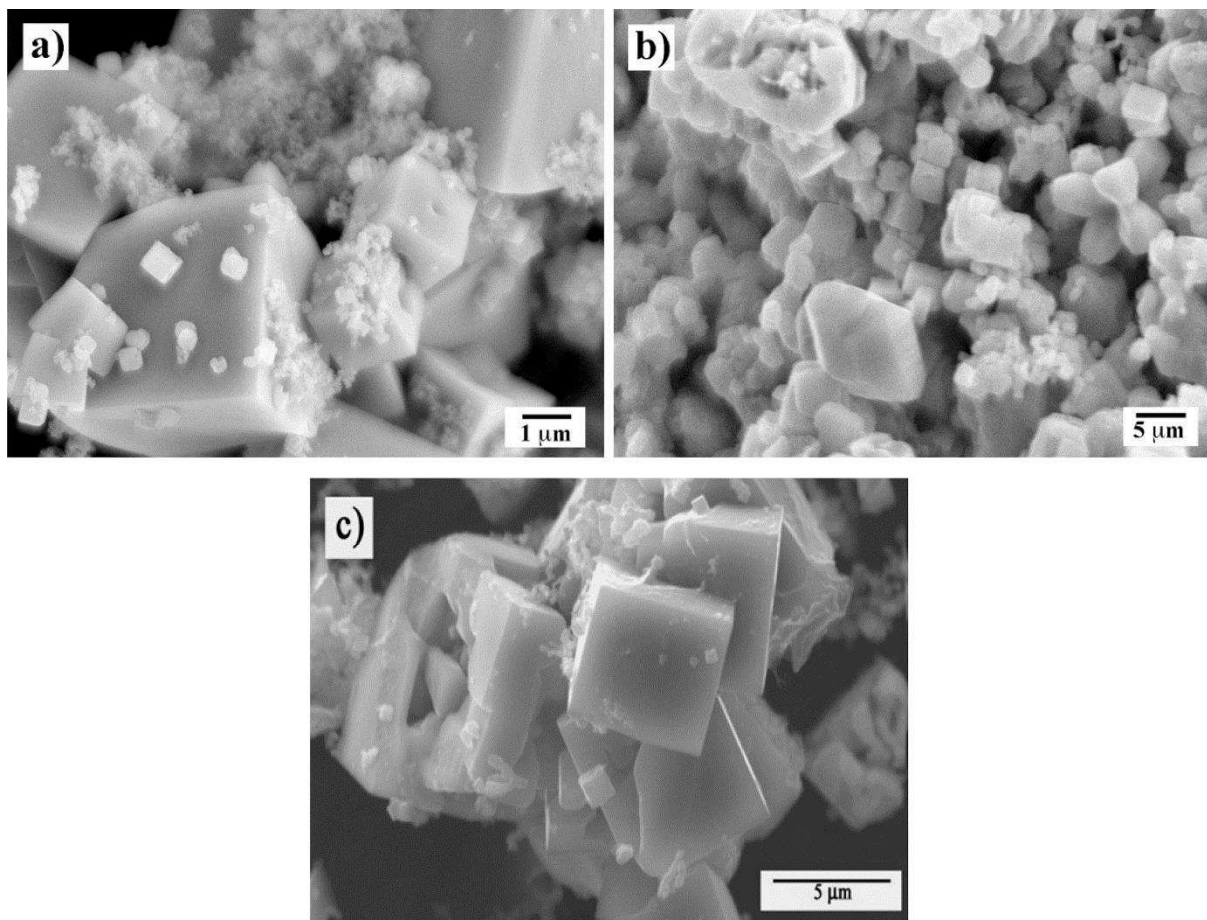
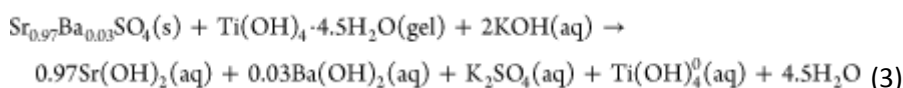
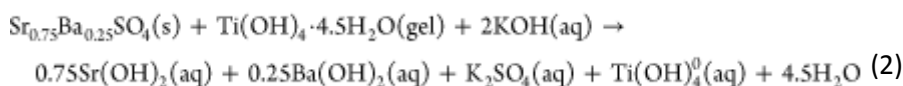


Figure 6. SEM images of the SrTiO₃ particles obtained after hydrothermal treatments of BC polycrystalline plates, conducted for 96 h in a 5 M KOH solution at (a) 150, (b) 200, and (c) 250 °C.

Variations on the particle morphology and size observed during the synthesis of SrTiO₃ are in good agreement with those previously reported for the hydrothermal preparation of BaTiO₃(38) and SrTiO₃(30) particles. Based in our results, we infer that the peculiar particle coarsening observed for longer reaction times and at higher temperatures may be promoted by intermediate dissolution–recrystallization of euhedral-like particles (dendritic and irregular) and the regular particles (cubic and star-shaped) obtained for early stages and temperatures below 200 °C, respectively. The marked SrTiO₃ particle growth was achieved by coarsening, following the Ostwald ripening mechanism(39) coupled with faceted particle growth.(40) This is supported by the fact that only a small fraction of fine particles remained at the treatments performed at temperatures above 200 °C.

3.4BC Polycrystalline Plate Single-Step Hydrothermal Conversion Pathway into SrTiO₃

The present results provide the first evidence regarding the feasibility of producing strontium titanate (SrTiO₃) using BC feedstock. The system, consisting of BC mineral and the Ti-gel, reacted to synthesize SrTiO₃ in alkaline media. This system is analogous to that for the formation of SrTiO₃ using only celestite, in which the mechanism of formation of the SrTiO₃ is achieved with the dissolution of celestite.(30)



Therefore, we surmise that the formation of SrTiO₃ from the conversion of the BC plate occurred according to the chemical reaction described by reaction 4, but this chemical equilibrium resulted from the simultaneous dissolution of the solid phases that is described by the chemical reactions given in reactions 2 and 3. The present transformation mechanism is different from that proposed for various single-step chemical reactions applied to prepare strontium and barium inorganic compounds using SrSO₄(28, 30) and BaSO₄(41) in highly concentrated alkaline hydrothermal media.

The reaction pathway associated with the synthesis of SrTiO₃ via the hydrothermal conversion of BC crystal plates was derived from SEM observations (see Figure 7). The SEM observation conducted on the raw BC polycrystalline plate shows a clear boundary between the two composing phases Sr_{0.75}Ba_{0.25}SO₄ and Sr_{0.97}Ba_{0.03}SO₄ (see Figure 7a). One of the BC plate cross section was exposed to the hydrothermal media, to ensure that both phases were in contact with

the alkaline media during the chemical reaction; this involved embedding the BC plate into the Ti-gel at the bottom of the autoclave. Visual observations indicated that the consumption of the BC crystal proceeded locally on the exposed surface and on those embedded into the Ti-gel. However, a heterogeneous dissolution was determined by the SEM observation of the partially reacted BC plate, indicating that the two initial solid phases had different chemical reactivities in the alkaline media. The partially reacted BC plate at 250 °C for 6 h consisted of aggregated euhedral crystals with an average size of 200 μm (see Figure 7b). Some small particles (100 μm average size) embedded in the euhedral crystals were also visible; the irregular bright areas were subjected to a severe corrosion process, as suggested by the eat pitch produced on their surfaces (Figure 7b). These observations slightly differ with the reaction pathway associated with the synthesis of SrTiO₃ using celestite crystals in 5 and 10 M NaOH.(30)

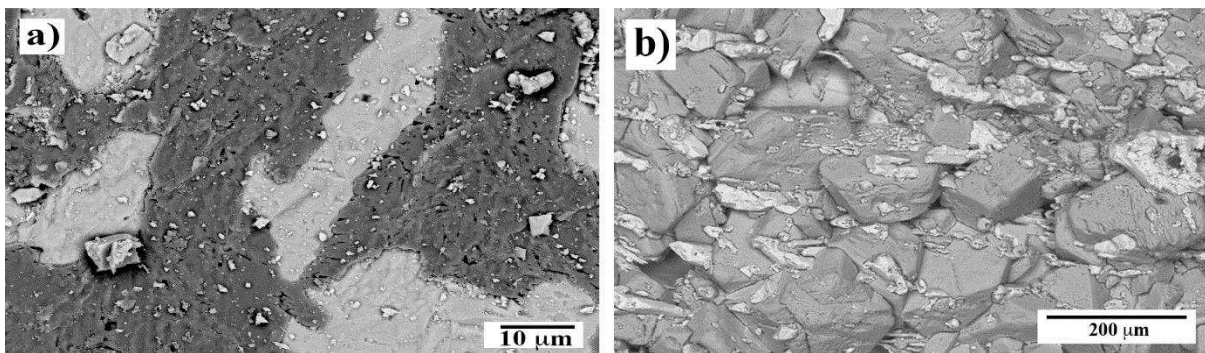


Figure 7. SEM images of (a) the BC polycrystalline plate surface without polish and (b) the partially converted BS plate at 250 °C for 6 h in a 5 M KOH solution.

EDX analyses conducted on the bright zones confirmed that these correspond to the Sr_{0.75}Ba_{0.25}SO₄ solid solution. The present results show clear evidence that indicate the global conversion process of the BC plate into the SrTiO₃ particles comprises the alternately dissolution of the solid phases as depicted by the chemical reactions described by reactions 2 and 3. At the early stage of the reaction, dissolution of the Sr_{0.75}Ba_{0.25}SO₄ phase occurred first, leading directly toward the chemical equilibrium described by reaction 4, resulting in the crystallization of a small amount of SrTiO₃. The rapid dissolution of this phase may be due to its high solubility in the alkaline 5 M KOH solution, realizing a reasonably high content of Ba to the hydrothermal media, as observed in the chemical quantification of the alkaline media (recall Figure 4). The continuous consumption of the Sr_{0.75}Ba_{0.25}SO₄ provoked a larger exposure of the emerged Sr_{0.97}Ba_{0.03}SO₄ crystals to the alkaline media, reacting next during an intermediate stage of the conversion (24–48 h). The predominant dissolution of both Sr_{0.97}Ba_{0.03}SO₄ and the remaining Sr_{0.75}Ba_{0.25}SO₄ phases over 24 h contributed to the extent of completion of the dissolution of the BC plate.

The dissolution pathway of BC polycrystalline plates has not been yet reported under alkaline hydrothermal conditions; however, our observations agree well with the dissolution of celestite

crystals to produce SrTiO₃.⁽³⁰⁾ Comparing the consumption of pure celestite and the BC plate at 250 °C in a 5 M KOH solution with the stoichiometric amount of Ti-gel for various reaction intervals (see Figure 8), we observed only a slightly larger consumption (α) of the BC plate, in comparison with that of the celestite crystal at the beginning of the reaction (6 h); this difference might be due to the rapid dissolution of Sr_{0.76}Ba_{0.25}SO₄. In contrast, the consumption of the BC crystal slightly slowed over 24 h, when the dissolution of the Sr_{0.97}Ba_{0.03}SO₄ initiated. Despite these differences, the results in Figure 7 provide evidence that the hydrothermal conversion of BC polycrystalline plates is consistent with the dissolution–crystallization mechanism involving the consumption of the precursor solid feedstock. Furthermore, the Ti-gel dehydration process occurring through the conversion may affect the scavenging of Sr²⁺ ions from the BC polycrystalline plate by the alkaline hydrothermal media. Under these reaction conditions, a particular steady state of reaction is achieved, which consists of the simultaneous formation of stoichiometric contents of aqueous Ti(OH)₄⁰ and aqueous Sr(OH)₂, according with reaction 4, leading spontaneously to the nucleation and growth of the SrTiO₃ particles. In our case, the crystallization of SrTiO₃ particles occurred preferentially at the Ti-gel surface and in the space between the partially consumed BC plates. The reaction concludes when the bulk dissolution of both BC and Ti-gel is completed; the detailed general scheme that is related to the present process is shown in Figure 9.

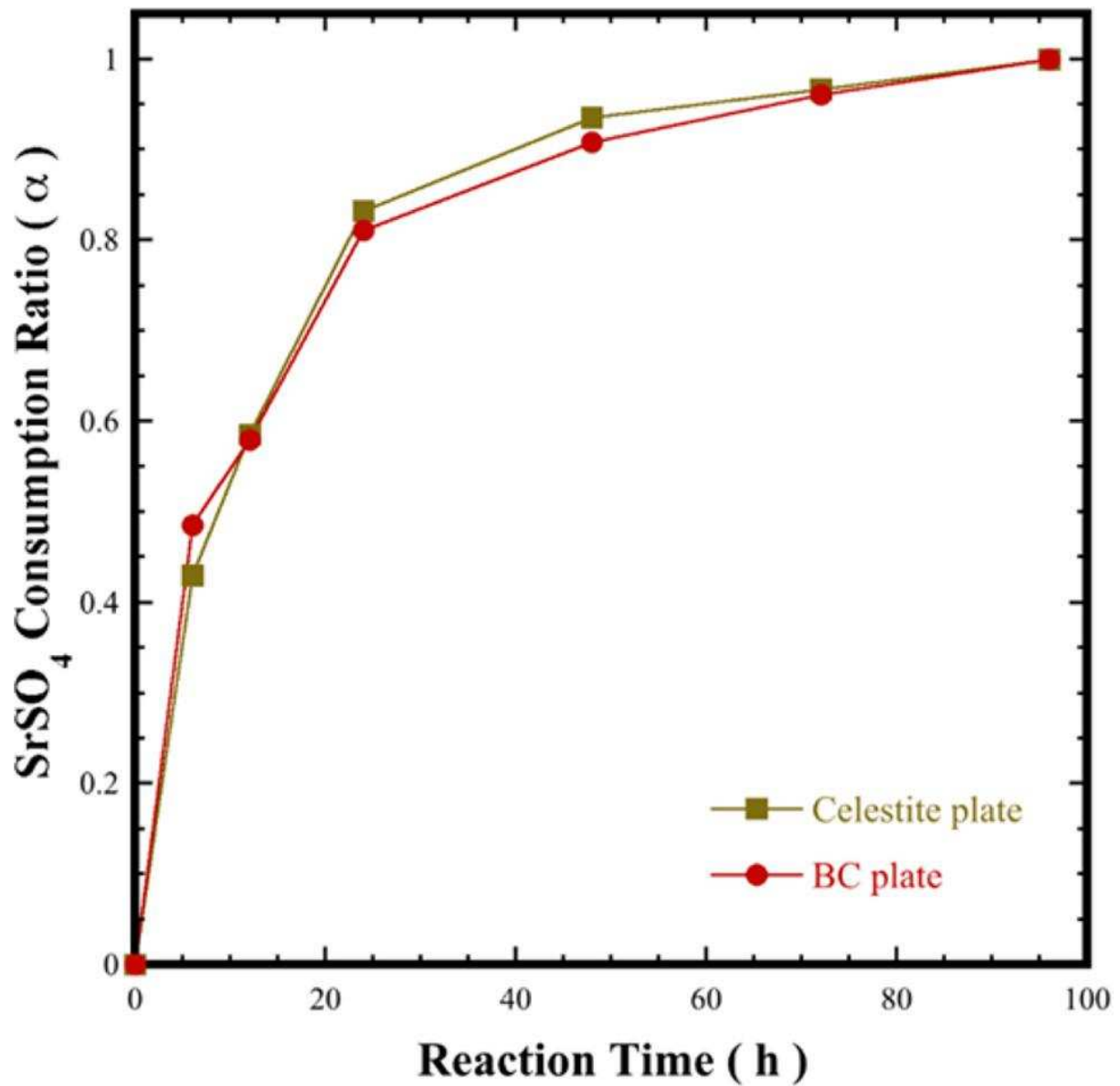


Figure 8. Consumption curves (α) of (■) pure celestite SrSO_4 and (●) the BC polycrystalline plates treated under hydrothermal conditions, using Ti-gel with a 5 M KOH solution for various reaction intervals at a temperature of 250 °C. All the treatments were conducted with an autoclave filling ratio of 40% for several reaction intervals.

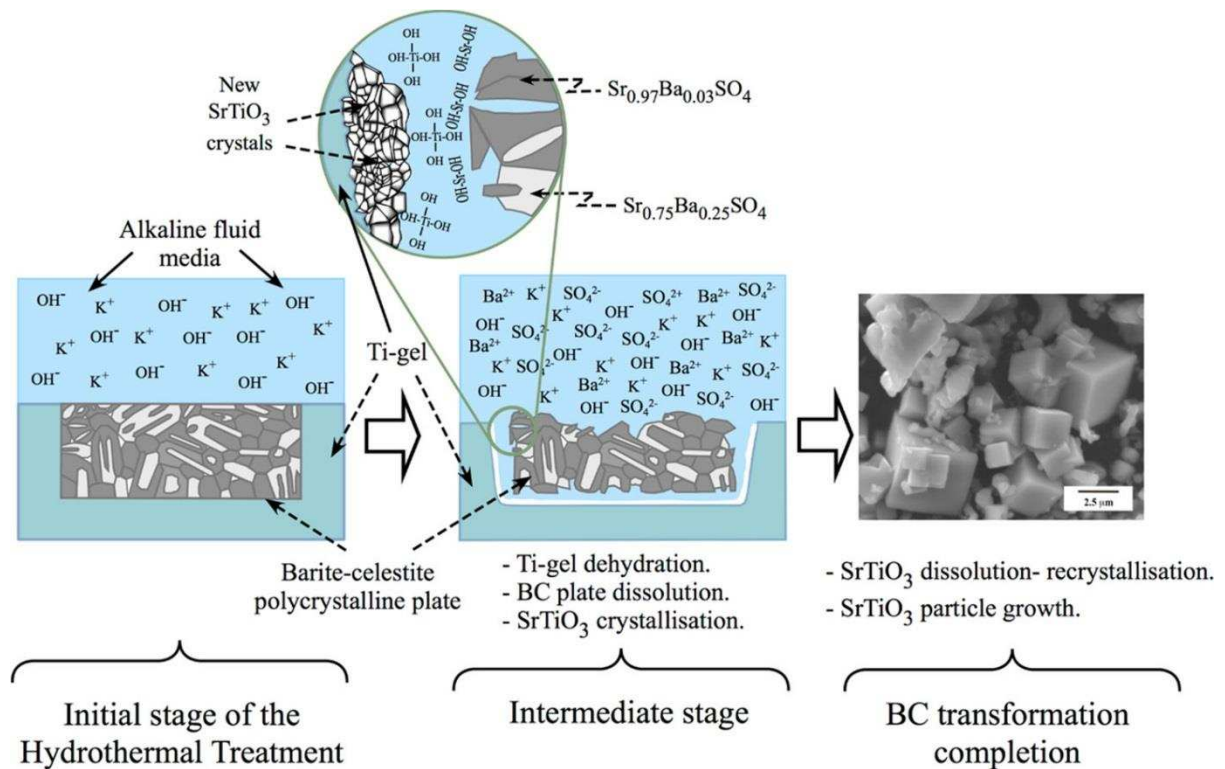


Figure 9. Scheme of the mechanism associated with the single-step transformation of BC plates into the crystallization of SrTiO_3 particle under hydrothermal conditions.

3.5 Kinetics of the Hydrothermal Conversion of BC Crystal Plates into SrTiO_3 Particles

The consumption ratio (α) of BC crystal plates was investigated under mild hydrothermal conditions in the temperature range between 150 and 250 °C. The hydrothermal conversion kinetics was evaluated using the consumption factor (α), as a function of the temperature parameter (see Figure 10a), since no other factors influence the kinetics of this reaction.⁽³⁰⁾ Our results indicate that the conversion of BC plates to SrTiO_3 occurred rapidly at mild temperatures of 200 and 250 °C for 24 h, reaching 56% ($\alpha = 0.56$) and 81% ($\alpha = 0.81$) consumption, respectively; however, the dissolution rate was slowed slightly for reaction intervals over 48 h. The full consumption of the BC plate ($\alpha = 1$) was achieved only for the longest reaction interval (96 h) at a temperature of 250 °C (see Figure 10a).

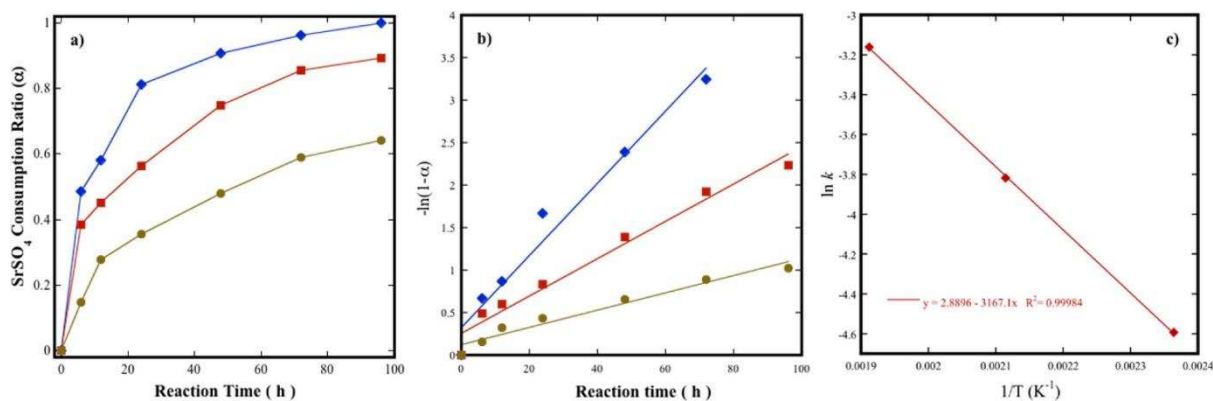


Figure 10. Consumption curves (α) of (a) BC polycrystalline plates treated under hydrothermal conditions in a 5 M KOH solution for various reaction intervals at different temperatures ((\bullet) 150, (\blacksquare) 200, and (\blacklozenge) 250 $^{\circ}\text{C}$). (b) Plot of the kinetic experimental data fitted with first-order function ($-\ln(1 - \alpha)$) against the time for different temperatures. (c) Arrhenius plot of the reaction rate against the reciprocal temperature associated with the first-order model.

The first-order kinetics model ($-\ln(1 - \alpha) = kt$) accurately fit the data ($R^2 = 0.95\text{--}0.97$; see Figure 10b), in contrast to other models tested, such as the second-order F2 and Jander's mathematical expression,(32) D3 ($(1 - (1 - \alpha)^{1/3})^2 = kt$, diffusion)(32) and D8 ($1 - (1 - \alpha)^{1/2})^2 = kt$, cylindrical diffusion)(32) that yielded lower R^2 values. Also, both the Johnson–Mehl–Avrami model(16, 38) and the new mathematical function derived from population balance approaches(42) were used to fit the present kinetic experimental data. However, these models led to lower R^2 values, indicating that the mechanism associated with each model does not apply to the current single-step transformation of SrTiO_3 particles. The constant rates were used to calculate the activation energy (E_a) required for the conversion of BC polycrystalline plates into SrTiO_3 powders. The E_a value obtained from the Arrhenius plot equation was $26.33 \text{ kJ mol}^{-1}$ (see Figure 10c); this value indicates that the one-step mechanism rate was controlled by the dissolution process at the solid/liquid interface, triggering the synthesis of SrTiO_3 . The E_a value associated with the BC plate transformation to SrTiO_3 particles is similar to those analogues of the single-step mineral hydrothermal conversion systems. In particular, celestite ore was employed as feedstock to synthesize SrTiO_3 (27.9 kJ mol^{-1}),(30) and SrWO_4 (27.2 kJ mol^{-1})(43) particles, under similar hydrothermal conditions used to treat the BC crystals. Furthermore, it has been reported that mechanical stirring may increase the rate of the conversion reaction, according to the results obtained in the transformation of SrSO_4 into SrWO_4 (18.3 kJ mol^{-1}),(44) was determined in recent research that was conducted by some of the current authors.(44)

One must emphasize that the barite–celestite mineral has a low commercial value, because of the high barium and calcium contents, which are present as major impurities. Currently, this mineral is only used to adjust the total barium content established for marketing by mixing it with SrSO_4 . Based on the present results, barite–celestite mineral has a great potential as a low-value mineral feedstock to the straightforward preparation of new functional oxide compounds (i.e.,

SrTiO₃). The transformation proceeds via a single-step chemical reaction under mild hydrothermal alkaline conditions. The process is economically attractive, in terms of the energy consumption, which is supported by the low activation energy required to achieve the transformation. Further experiments would be required to evaluate the treatment of the primary waste (a K₂SO₄–KOH solution) to reduce the potential harm of this effluent to the environment; one economically way to dispose of this solution would involve an acid neutralization coupled with the liquid evaporation to K₂SO₄, which can be used as fertilizer.

4 Conclusions

Barite–celestite (BC) mineral exhibits appropriate chemical reactivity to promote the synthesis of SrTiO₃ under alkaline hydrothermal conditions, similar to that observed when using high-purity and expensive chemical reagents. The reaction temperature was the main factor that achieved the transformation of BC plate to SrTiO₃ to full completion in a single-step reaction. Under hydrothermal conditions, the complete conversion occurred in a 5 M KOH solution at 250 °C after 96 h. The synthesis of SrTiO₃ particles is mainly achieved by a dissolution–precipitation mechanism, which is initially triggered by the dissolution of the Sr_{0.75}Ba_{0.25}SO₄ phase and the simultaneous dehydration of the Ti-gel. Subsequently, the dissolution of Sr_{0.97}Ba_{0.03}SO₄ occurs to accomplish the total transformation of both phases toward the synthesis of SrTiO₃ particles. A variation in the morphology of the SrTiO₃ particles was promoted by increasing both reaction interval and temperature. The preferential crystallization of submicrometer-sized SrTiO₃ particles with irregular and dendritic shapes occurred at early and intermediate reaction intervals below 200 °C. The growth stage of cubic-shaped particles is purely controlled by the Oswald ripening coarsening mechanism, coupled with a faceted growth process, producing agglomerates with an average size of 20 μm. This mechanism is achieved through a secondary reaction involving a SrTiO₃ dissolution–recrystallization process that occurs at >200 °C over a period of 48 h. Overall, the transformation is a low-energy (26.33 kJ mol⁻¹) process which is economically attractive to produce a functional material that is widely used in the electronics industry.

The authors declare no competing financial interest.

Acknowledgment

The present work was supported by the research grant Nos. FOMIX-COAH 2003-C02-02 and CONACYT-MEXICO CB-2008-01-0107052. Three of the authors—J.C.R.A., Z.M.V., R.P.G., and J.L.R.G.—are indebted to the CONACYT-SNI. J.C.R.A. is indebted for the financial support in the form of a Sabbatical research grant to conduct part of this work. Many thanks are also given to Eng. Felipe Marquez at CINVESTAV-IPN Campus Saltillo, México, for his assistance with the scanning electron microscopy observations.

References

1. Liu, X.; Bai, H. Liquid-solid reaction synthesis of SrTiO₃ submicron-sized particles Mater. Chem. Phys. **2011**, 127, 21 DOI: 10.1016/j.matchemphys.2011.01.056
2. Huang, S. T.; Lee, W. W.; Chang, J. L.; Huang, W. S.; Chou, S. Y.; Chen, C. C. Hydrothermal synthesis of SrTiO₃ nanocubes: Characterization, photocatalytic activities, and degradation pathway J. Taiwan Inst. Chem. Eng. **2014**, 45, 1927 DOI: 10.1016/j.jtice.2014.02.003
3. Shen, H.; Lu, Y.; Wang, Y.; Pan, Z.; Cao, G.; Yan, X.; Fang, G. Low temperature hydrothermal synthesis of SrTiO₃ nanoparticles without alkali and their effective photocatalytic activity J. Adv. Ceram. **2016**, 5 (4) 298 DOI: 10.1007/s40145-016-0203-3
4. Ishikawa, H.; Oohira, K.; Nakajima, T.; Akiyama, T. Combustion synthesis of SrTiO₃ using different raw materials J. Alloys Compd. **2008**, 454, 384 DOI: 10.1016/j.jallcom.2006.12.113
5. Zheng, Z.; Huang, B.; Qin, X.; Zhang, X.; Dai, Y. Facile Synthesis of SrTiO₃ hollow microspheres built as assembly of nanocubes and their associated photocatalytic activity J. Colloid Interface Sci. **2011**, 358, 68 DOI: 10.1016/j.jcis.2011.02.032
6. Bacha, E.; Deniard, P.; Richard-Plouet, M.; Brohan, L.; Gundel, H. W. An inexpensive and efficient method for the synthesis of BTO and STO at temperatures lower than 200 °C Thin Solid Films **2011**, 519, 5816 DOI: 10.1016/j.tsf.2010.12.190
7. Zhang, Z.; Zhao, L.; Wang, X.; Yang, J. The preparation and electrical properties of SrTiO₃-based capacitor–varistor double-function ceramics J. Sol-Gel Sci. Technol. **2004**, 32, 367 DOI: 10.1007/s10971-004-5819-z
8. Liu, Y.-F.; Lu, Yi-N.; Xu, M.; Zhou, L.-F.; Shi, S.-Z. Topochemical reaction of SrTiO₃ platelet crystals based on Sr₃Ti₂O₇ platelet precursor in molten salt synthesis process Mater. Chem. Phys. **2009**, 114, 37 DOI: 10.1016/j.matchemphys.2008.05.101
9. Li, H.-L.; Du, Z.-N.; Wang, G.-L.; Zhang, Y.-C. Low temperature molten salt synthesis of SrTiO₃ submicron crystallites and nanocrystals in the eutectic NaCl–KCl Mater. Lett. **2010**, 64, 431 DOI: 10.1016/j.matlet.2009.11.040
10. Wang, T. X.; Liu, S.-Z.; Chen, J. Molten salt synthesis of SrTiO₃ nanocrystals using nanocrystalline TiO₂ as a precursor Powder Technol. **2011**, 205, 289 DOI: 10.1016/j.powtec.2010.08.068
11. Kim, K. H.; Park, J. K.; Kim, C. H.; Park, H. D.; Chang, H.; Choi, S. Y. Synthesis of SrTiO₃: Pr, Al by ultrasonic spray pyrolysis Ceram. Int. **2002**, 28, 29 DOI: 10.1016/S0272-8842(01)00054-2
12. Kuang, Q.; Yang, S. Template synthesis of single-crystal-like porous SrTiO₃ nanocube assemblies and their enhanced photocatalytic hydrogen evolution ACS Appl. Mater. Interfaces **2013**, 5, 3683 DOI: 10.1021/am400254n

13. Rabuffetti, F. A.; Kim, H.-S.; Enterkin, J. A.; Wang, Y.; Lanier, C. H.; Marks, L. D.; Poepelmeier, K. R.; Stair, P. C. Synthesis-dependent first-order Raman scattering in SrTiO₃ nanocubes at room temperature *Chem. Mater.* **2008**, 20, 5628 DOI: 10.1021/cm801192t
14. Chen, L.; Zhang, S.; Wang, L.; Xue, D.; Yin, S. Preparation and photocatalytic properties of strontium titanate powders via sol–gel process *J. Cryst. Growth* **2009**, 311, 746 DOI: 10.1016/j.jcrysgro.2008.09.185
15. Zorel, H. E.; Guinesi, L. S.; Ribeiro, C. A.; Crespi, M. S. SrTiO₃ preparation through coprecipitation methods *Mater. Lett.* **2000**, 42, 16 DOI: 10.1016/S0167-577X(99)00152-4
16. Walton, R. I.; Millange, F.; Smith, R. I.; Hansen, T. C.; O'Hare, D. Real time observation of the hydrothermal crystallization of barium titanate using in situ neutron powder diffraction *J. Am. Chem. Soc.* **2001**, 123, 12547 DOI: 10.1021/ja011805p
17. Zhu, H.; Gao, X.; Lan, Y.; Song, D.; Xi, Y.; Zhao, J. Hydrogen titanate nanofibers covered with anatase nanocrystals: A delicate structure achieved by the wet chemistry reaction of the titanate nanofibers *J. Am. Chem. Soc.* **2004**, 126, 8380 DOI: 10.1021/ja048204t
18. Chen, D.; Jiao, X.; Zhang, M. Hydrothermal synthesis of strontium titanate powders with nanometer size derived from different precursors *J. Eur. Ceram. Soc.* **2000**, 20, 1261 DOI: 10.1016/S0955-2219(00)00003-0
19. Zhang, S.; Liu, J.; Han, Y.; Chen, B.; Li, X. Formation mechanisms of SrTiO₃ nanoparticles under hydrothermal conditions *Mater. Sci. Eng., B* **2004**, 110, 11 DOI: 10.1016/j.mseb.2004.01.017
20. Wang, H.; Zhao, W.; Zhang, Y.; Zhang, S.; Wang, Z.; Zhao, D. A facile in-situ hydrothermal synthesis of SrTiO₃/TiO₂ microsphere composite *Solid State Commun.* **2016**, 236, 27 DOI: 10.1016/j.ssc.2016.03.003
21. Jayabal, P.; Sasirekha, V.; Mayandi, J.; Jeganathan, K.; Ramakrishnan, V. A facile hydrothermal synthesis of SrTiO₃ for dye sensitized solar cell application *J. Alloys Compd.* **2014**, 586, 456 DOI: 10.1016/j.jallcom.2013.10.012
22. Zhang, Y.; Zhong, L.; Duan, D. Single-step hydrothermal synthesis of strontium titanate nanoparticles from crystalline anatase titanium dioxide *Ceram. Int.* **2015**, 41, 13516 DOI: 10.1016/j.ceramint.2015.07.145
23. Kim, M.; Hong, S. A.; Shin, N.; Lee, Y. H.; Shin, Y. Synthesis of strontium titanate nanoparticles using supercritical water *Ceram. Int.* **2016**, 42, 17853 DOI: 10.1016/j.ceramint.2016.08.120
24. Maxim, F.; Ferreira, P.; Vilarinho, P. M.; Reaney, I. Hydrothermal synthesis and crystal growth studies of BaTiO₃ using Ti nanotube precursors *Cryst. Growth Des.* **2008**, 8 (9) 3309 DOI: 10.1021/cg800215r

25. Zhang, S.; Han, Y.; Chen, B.; Song, X. The influence of TiO₂-H₂O gel on hydrothermal synthesis of SrTiO₃ powders Mater. Lett. **2001**, 51, 368 DOI: 10.1016/S0167-577X(01)00345-7
26. Li, J.; Luo, S.; Alim, M. A. The role of TiO₂ powder on the SrTiO₃-based synthesized varistor materials Mater. Lett. **2006**, 60, 720 DOI: 10.1016/j.matlet.2005.09.070
27. Suárez-Orduña, R.; Rendón-Angeles, J. C.; López-Cuevas, J.; Yanagisawa, K. The conversion of mineral celestite to strontianite under alkaline hydrothermal conditions J. Phys.: Condens. Matter **2004**, 16, S1331 DOI: 10.1088/0953-8984/16/14/046
28. Suárez-Orduña, R.; Rendón-Angeles, J. C.; Matamoros-Veloza, Z.; Yanagisawa, K. Exchange of SO₄²⁻ ions with F⁻ ions in mineral celestite under hydrothermal conditions Solid State Ionics **2004**, 172, 393 DOI: 10.1016/j.ssi.2004.03.022
29. Rendón-Angeles, J. C.; Pech-Canul, M. I.; López-Cuevas, J.; Matamoros-Veloza, Z.; Yanagisawa, K. Differences on the conversion of celestite in solutions bearing monovalent ions under hydrothermal conditions J. Solid State Chem. **2006**, 179, 3645 DOI: 10.1016/j.jssc.2006.07.043
30. Rangel-Hernandez, Y. M.; Rendon-Angeles, J. C.; Matamoros-Veloza, Z.; Pech-Canul, M. I.; Diaz-de la Torre, S.; Yanagisawa, K. One-step synthesis of fine SrTiO₃ particles using SrSO₄ ore under alkaline hydrothermal conditions Chem. Eng. J. **2009**, 155, 483 DOI: 10.1016/j.cej.2009.07.024
31. Hanor, J. S. Frequency distribution of compositions in the barite–celestite series Am. Mineral. **1968**, 53 (6) 1215
32. Markus, H.; Fugleberg, S.; Valtakari, D.; Salmi, T.; Murzin, D. Y.; Lahtinen, M. Kinetic modelling of a solid–liquid reaction: reduction of ferric iron to ferrous iron with zinc sulphide Chem. Eng. Sci. **2004**, 59, 919 DOI: 10.1016/j.ces.2003.10.022
33. Aydogan, S.; Aras, A.; Canbazoglu, M. Dissolution kinetics of sphalerite in acidic ferric chloride leaching Chem. Eng. J. **2005**, 114, 67 DOI: 10.1016/j.cej.2005.09.005
34. Sczancoski, J. C.; Cavalcante, L. S.; Joya, M. R.; Espinosa, J. W. M.; Pizani, P. S.; Varela, J. A.; Longo, E. Synthesis, growth process and photoluminescence properties of SrWO₄ powders J. Colloid Interface Sci. **2009**, 330, 227 DOI: 10.1016/j.jcis.2008.10.034
35. Sczancoski, J. C.; Bomio, M. D. R.; Cavalcante, L. S.; Joya, M. R.; Pizani, P. S.; Varela, J. A.; Longo, E.; Li, M. S.; Andrés, J. A. Morphology and blue photoluminescence emission of PbMoO₄ processed in conventional hydrothermal J. Phys. Chem. C **2009**, 113, 5812 DOI: 10.1021/jp810294q
36. Mourão, H. A. J. L.; Lopes, O. F.; Ribeiro, C.; Mastelaro, V. R. Rapid hydrothermal synthesis and pH-dependent photocatalysis of strontium titanate microspheres Mater. Sci. Semicond. Process. **2015**, 30, 651 DOI: 10.1016/j.mssp.2014.09.022
37. Lencka, M. M.; Riman, R. E. Thermodynamic modelling of hydrothermal synthesis of ceramic powders Chem. Mater. **1993**, 5 (1) 61 DOI: 10.1021/cm00025a014

38. Moon, J.; Suvaci, E.; Morrone, A.; Costantino, S. A.; Adair, J. H. Formation mechanisms and morphological changes during the hydrothermal synthesis of BaTiO₃ particles from chemically modified, amorphous titanium (hydrous) oxide precursor J. Eur. Ceram. Soc. **2003**, 23, 2153 DOI: 10.1016/S0955-2219(03)00016-5
39. Peterson, C. R.; Slamovich, E. B. Effect of processing parameter on the morphology of hydrothermally derived PbTiO₃ powders J. Am. Ceram. Soc. **1999**, 82 (7) 1702 DOI: 10.1111/j.1151-2916.1999.tb01989.x
40. Berge, B.; Faucheux, L.; Schwab, K.; Libchaber, A. Faceted crystal growth in two dimensions Nature **1991**, 350, 322 DOI: 10.1038/350322a0
41. Rendón-Angeles, J. C.; Matamoros-Veloza, Z.; López-Cuevas, J.; Pech-Canul, M. I.; Yanagisawa, K. Stability and direct conversion of mineral Barite crystals in carbonated hydrothermal fluids J. Mater. Sci. **2008**, 43, 2189 DOI: 10.1007/s10853-007-2044-5
42. Testino, A.; Buscaglia, V.; Buscaglia, M. T.; Viviani, M.; Nanni, P. Kinetic modelling of aqueous and hydrothermal synthesis of barium titanate (BaTiO₃) Chem. Mater. **2005**, 17 (21) 5346 DOI: 10.1021/cm051119f
43. Rendón-Angeles, J. C.; Matamoros-Veloza, Z.; López-Cuevas, J.; Gonzalez, L. A.; Montoya-Cisneros, K. L.; Yanagisawa, K.; Willis-Richards, J.; Diaz-Algara, J. Rapid synthesis of scheelite SrWO₄ particles using a natural SrSO₄ ore under alkaline hydrothermal conditions Hydrometallurgy **2015**, 157, 116 DOI: 10.1016/j.hydromet.2015.07.019
44. Rendón-Angeles, J. C.; Matamoros-Veloza, Z.; López-Cuevas, J.; Perez-Garibay, R.; Diaz-Algara, J.; Yanagisawa, K. Rotary-hydrothermal method assisting the conversion of celestine into scheelite SrWO₄ in alkaline solutions Int. J. Miner. Process. **2016**, 148, 105 DOI: 10.1016/j.minpro.2016.01.022